Special Section on EuroVA 2021

Understanding multi-modal brain network data: An immersive 3D visualization approach

Britta Pester [a,*], Benjamin Russig [a], Oliver Winke [a], Carolin Ligges [b], Raimund Dachselt [c,d,e], Stefan Gumhold [a,d,e]

[a] Chair for Computer Graphics and Visualization, TU Dresden, Germany
[b] Jena University Hospital, Department of Child and Adolescent Psychiatry, Psychosomatic Medicine and Psychotherapy, Friedrich Schiller University Jena, Germany
[c] Interactive Media Lab Dresden, TU Dresden, Germany
[d] Centre for Tactile Internet with Human-in-the-Loop (CeTI), TU Dresden, Germany
[e] Cluster of Excellence Physics of Life, TU Dresden (PoL), Germany

ARTICLE INFO

ABSTRACT

Understanding the human brain requires the incorporation of functional interaction patterns that depend on a variety of features like experimental setup, strength of directed connectedness or variability between several individuals or groups. In addition to these external factors, there are internal properties of the brain network as for example temporal propagation of connections, or connectivity patterns that only occur in a distinct frequency range of the signal. The visualization of detected networks covering all necessary information poses a substantial problem which is mainly due to the high number of features that have to be integrated within the same view in a natural spatial context.

To address this problem, we propose a new tool that transfers the network into an anatomically arranged origin–destination view in a virtual visual analysis lab. This offers the user an opportunity to assess the temporal evolution of connectivity patterns and provides an intuitive and motivating way of exploring the corresponding features via navigation and interaction in virtual reality (VR). The approach was evaluated in a user study including participants with neuroscientific background as well as people working in the field of computer science. As a first proof of concept trial we used functional brain networks derived from time series of electroencephalography recordings evoked by visual stimuli. All participants gave a positive general feedback, notably they saw a benefit in using the VR view instead of the compared 2D desktop variant. This suggests that our application successfully fills a gap in the visualization of high-dimensional brain networks and that it is worthwhile to further follow and enhance the proposed representation method.

1. Introduction

The field of experimental and clinical neuroscience is constantly gaining importance [1]. While methods for the analysis of brain anatomy or brain-behavior relationships improve, large parts of the functionalities of the human brain are yet to be discovered. In particular, the investigation of directed information transfer within the human brain is a growing field of research. Understanding how the components of these complex neural networks within the human brain interact and affect each other is essential to understand and treat various different neurological, mental or developmental disorders [2–4].

Interaction and inter-connectivity of neurons or brain regions is called brain connectivity and can be separated into three categories [5]: *structural connectivity* refers to concrete neuroanatomical connections, *functional connectivity* describes the temporal correlations between neurophysiological events of spatially neighboring or remote neuronal structures and finally, *effective connectivity* is defined as the directed influence of one neuronal structure on another, mediated directly or indirectly. Amongst others, the networks can be derived from various neurophysiological recording techniques such as electroencephalography (EEG), magnetoencephalography, positron emission tomography and functional magnetic resonance imaging [6,7].

* Corresponding author.
  E-mail addresses: britta.pester@tu-dresden.de (B. Pester), benjamin.russig@tu-dresden.de (B. Russig), oliver.winke@tu-dresden.de (O. Winke), carolin.ligges@med.uni-jena.de (C. Ligges), raimund.dachselt@tu-dresden.de (R. Dachselt), stefan.gumhold@tu-dresden.de (S. Gumhold).

Within the last few years, the combination of simultaneously recorded EEG and fMRI data has received growing interest in studying neural activity and, still more recently, also for the investigation of neural connectivity [8,9].

In our work, we focus on functional connectivity derived from the analysis of EEG time series data. Here, it is assumed that the underlying functional brain connectivity patterns possess a certain strength and direction of neural information transfer. They are thus considered as so-called *weighted, directed* networks. Additionally, these networks contain information with respect to several *modes*. . The mode space indicates the location of possibly occurring directed connections within the brain (i.e. position of electrodes on the scalp). Consequently, this information includes the anatomical context of information transfer within the brain network. Temporal evolution of the functional connections is integrated via the mode time, which is of particular interest when it can be expected that the network is undergoing change in the course of a cognitive task. Finally, the mode frequency must be considered, too, as electrical brain activity is characterized by typical frequency ranges (also known as frequency bands) of brain activation that show different properties depending on a mental state or cognitive task. These frequency-dependent variations do not only occur in brain activation but also in functional brain connectivity [10]. Without any further processing, however, the understanding of resulting brain networks comprising all three modes at once is impossible. A graphical representation can offer a useful tool in this situation, yet the effective and intuitive visualization of such multi-dimensional data remains a major challenge. Current solutions mainly rely on (1) spatial context by showing aggregated or reduced data, or (2) crowded abstract visualizations [11,12]. Regarding (1), aggregation leads to a loss of detail and the outcome depends on the parameters the data are aggregated upon (e.g. mean across time or mean within a distinct frequency band). Data reduction achieved by a preselection of displayed electrodes has the disadvantage that the overall view on the brain network as a whole gets lost. Regarding (2), abstract matrix-like visualizations can integrate time and frequency dimensions of the complex data, but they lose the spatial context making it less intuitive and more difficult to understand.

In order to counteract these limitations, we propose a visualization tool with the goal to fulfill the following five requirements R1, . . ., R5. The approach should

- (R1) allow a view on the whole weighted, directed network comprising all EEG electrodes,
- (R2) keep the anatomical context to offer an intuitive understanding of brain networks,
- (R3) visualize the propagation of connectedness over time,
- (R4) integrate various frequency ranges and
- (R5) additionally offer the possibility for the application of individual, case-specific restrictions (e.g. choice of certain brain areas or thresholds for minimum connectivity strength of displayed connections).

Finally, the general demand beyond all these requests must be to provide an efficient inclusion of all aspects listed above in order to make the overall perception of the complex visualization as intuitive and understandable as possible.

To achieve this goal we propose a novel visual analysis tool in a 3D immersive virtual reality (VR) environment. Electrodes are displayed in an anatomical arrangement across the human scalp and the temporal evolution of directed interaction is color-coded by the edge weights within the brain network. That means, in contrast to conventional visualization approaches, the color of the 3D links between brain areas changes along the length of the edges. Interaction opportunities like selection of distinct EEG electrodes or filtering via switching between different edge weight thresholds offer the possibility to adaptively visualize the data and enhance spatial perception of appearing patterns within the brain network. Notably the application offers an effective way of a non-hypothesis-driven exploration of brain connectivity: Regions of interest regarding any of the dimensions space, time and frequency do not have to be known a priori and can be explored via the immersive 3D view, helping to generate new hypotheses which had not been in the focus of neuroscientific research yet.

This work is an extended version of the conference paper *"Immersive 3D Visualization of Multi-Modal Brain Connectivity"* [13].

2. Related work

Visualization of brain connectivity. From a user perspective, the graphical illustration of brain networks is merely an instrument for visually exploring observed connectivity patterns. From a developer's point of view, the focus is on an appropriate design and the graphical realization. Triggered by discussion between neuroscientists and experts in graphical visualization, Kuhlen and Hentschel propose an interactive tool that joins abstract matrix-like representations together with comprehensive 3D visualizations in form of node-link diagrams [14]. In [6], several techniques for the graphical representation of connectomics, including the visualization of anatomical connections among neurons as well as static functional networks as for example derived from correlation analysis. For the most part, existing network visualization tools do not offer or insufficiently offer the possibility to include a high number of available properties (modes). A common solution to this problem is the reduction of visualized content. This can be achieved by restricting the view to a hypothesis-driven preselection of cortical region/time interval/frequency band, or a previous agglomeration of data [11]. Another well-established approach is to apply methods from graph theory in order to segregate the network into brain regions with similar topological properties [12].

Origin–destination flow visualization. The main goal of spatially arranged origin–destination (OD) flow maps is to show connections within a network corresponding to locations in space [15,16]. That means, the above stated demand for an intuitive representation of spatial constellations within the network is absolutely fulfilled (R2). In the case where the sample of origins (*sources*) is the same as those of destinations (*sinks*), a commonly adapted visualization approach is to duplicate the map. One map represents the sources of information transfer and the other one represents the sink of information transfer. An artificial example is shown in Fig. 1. In 1(a), the network comprising five network nodes is drawn in the form of a 2D node-link diagram. All connections (network edges) are represented by directed arrows between the network nodes. In contrast, the OD representation in 1(b) shows the network in form of two reference spaces, separating the network into a set of sink nodes and one of source nodes. The network nodes of 1(a) and (b) correspond to each other, which is indicated by the respective color.

A possibility to include the aspect of temporally varying information flow (R3) is proposed in [17], where the connected lines between the locations are interrupted by heatmaps that represent the temporal evolution of connections from each individual source to all possible sinks. This brings the strong benefit of supporting the time-dependent evolution of networks but comes with the disadvantage that the number of drawn heatmaps increases quadratically with the locations in the network, impairing the ad-hoc readability. The *MapTrix* visualization [18] omits drawing all possible connections in the visualization, by combining the origin and the destination map with a corresponding adjacency matrix that encodes the strength of connectedness
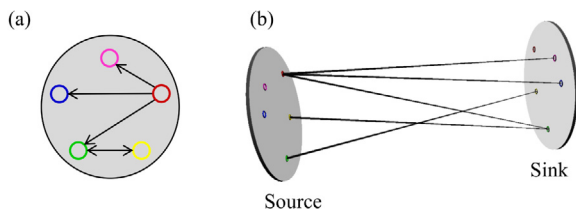
Fig. 1. Visualization of a synthetic five-node network. In subfigure (a), a directed network containing $D = 5$ nodes is shown. (b) provides the corresponding OD visualization.

between source and sink location. Again, the readability of the visualization is affected by this combined view. On the other hand, the complete weighted network can be offered (R1).

Immersive visualizations. Immersive visualizations have been explored for many data types like 3D graph layouts [19–21], multivariate data [22], or even multi-user applications on wall-displays [23]. Yang et al. presented a method for the immersive visualization of OD data. Several representations of geographic flow maps are introduced and compared with the final conclusion that the 3D view should be preferred to the 2D alternative [24]. In [25], the authors survey the VR visualization of large graphs with the main focus on the navigation through these high-dimensional 3D networks and the comparison of various immersive navigation techniques. The impact of a rising level of immersion is examined in [26] where participants had the task to identify ground truth clusters within a 2D or 3D scatter plot respectively. The varying degree of immersion was included by offering a 2D view on screen and a 3D view on screen as well as a miniature 3D view in VR and room-scaled 3D view in VR. Furthermore the authors carefully investigated additional influence by further aspects such as added noise and different cluster properties. With regard to various output variables such as error rate or subjective preference, all 3D variants (including the 3D screen view) outperform the 2D variant by far. Furthermore, the 3D screen view is less beneficial than both VR versions — yet, this difference is not very pronounced [26]. All of these approaches have the great benefit of intuitive recognition in space (R2), together with the possibility of case-specific interaction by the user (R5).

To our knowledge, the only tool that allows for an immersive visualization of functional brain connectivity data is *NeuroCave*, a web-based VR application for analyzing the human connectome [27,28]. The tool provides several spatial and abstract views of the (non-directed) functional connectivity graph which can be displayed and navigated either on a regular display or in VR. They found that the latter greatly enhanced general user engagement with exploring the data. In contrast to the non-immersive mode, it was additionally easier for the users to come up with hypotheses which they preferred to investigate further. This user assessment clearly supports our plan to utilize an immersive VR framework for reaching the goal of an intuitive, motivating and explorative way of investigating the highly complex brain networks. However, the application has some limitations. First, this tool does not support weighted, directed network edges (R1), as the only option for indicating connections within the network is to draw linking lines between pairs of network nodes. This dichotomous way of network visualization implies a loss of information about strength and direction of information transfer. Furthermore, the previously described additional data features like time and frequency (R3, R4) cannot be integrated in the views the tool provides.

Contribution of the new tool. The literature provided above is an excerpt of current approaches for dealing with distinct

aspects of network visualization. Any of them either fulfills a certain subset of the requirements R1, . . ., R5 by nature, or the methods can be adapted in such way that distinct requirements of current interest are met. However, neither approach meets all five criteria at the same time. As already mentioned in the introductory paragraph, any of the demands R1, . . ., R5 renders an essential aspect of the complete network. Disregarding some of them entails a loss of possibly relevant information. This is the reason why we specifically propose a tool that offers a visualization that *combines the entire set* of requirements, allowing an in-depth understanding of brain connectivity patterns without losing information that is actually available.

3. Processing concept

Any visualization tool has to be realized in consideration of the data type that has to be illustrated as well as the research questions that have to be answered. The goal of the application presented here is to visualize multi-modal brain networks derived from EEG data. More precisely, the research question posed by the data is the identification of functionally connected brain regions during visual stimuli processing.

In this section, the cascade of involved processing steps will be introduced. We begin with the description of recorded EEG data and the applied methodology for the subsequent calculation of EEG-based brain networks. Then, the components of our new visualization tool will be presented, followed by an outline of the possibilities for the offered user interactions.

3.1. EEG-based brain connectivity

Raw data (EEG time series). We worked with EEG data from an experiment investigating visual evoked potentials [29]. $K = 40$ visual stimuli were presented for 1100 ms each and were then segmented into $K = 40$ trials lasting from 500 ms before and 1100 ms after the stimulus onset. For the recording, we used the international 10/20 system, a commonly applied scheme for the standardized arrangement of EEG electrodes on the scalp [30,31]. According to that system, $D = 28$ active EEG electrodes have been placed together with two additional reference channels as well as three channels to register eye movement. As a preprocessing step, time series were sampled down to 125 Hz in time resulting in $N = 201$ temporal samples [32]. By using that diminished sampling rate, data size is reduced, whilst all frequency bands which have been found to be relevant for the analysis of visual evoked potentials are still covered [33,34].

Derived data (functional brain networks). The described EEG time series provide an example where multiple features necessarily have to be included into network analysis [35]. First, connectivity may have a spatial focus and direction on the scalp. Second, temporal variation of the experiment arising from the presented stimuli of the study protocol requires a time-variant network analysis. Third, network patterns have to be analyzed depending on frequency bands. For this type of data, time-variant multivariate autoregressive models (tvMVAR) provide an appropriate basis for the quantification of connectivity within the network [36]. We therefore applied the following strategy for the quantification of multi-modal brain connectivity data.

In the first step, time series are approximated by means of tvMVAR modeling. A univariate time series $[y(1), \ldots, y(N)] \in \mathbb{R}^N$ is a vector of N scalar EEG observations at equidistant distributed samples in time. EEG is recorded simultaneously at D locations (EEG electrodes) and K repetitions of the presented visual stimulus (trials of the experiment), resulting in a multivariate $K \times D \times N$-dimensional time-series tensor containing the segmented stimuli. The time series is approximated by an

$(N − p) × D$-dimensional tvMVAR process of order p which is defined by [37]:

$$Y(n) = \sum_{r=1}^{p} \mathbf{A}^r(n)Y(n − r) + E(n), \ n = p + 1, \ldots, N.$$

$\mathbf{A}^r(n) \in \mathbb{R}^{D\times D}$ are the temporally varying autoregressive parameter matrices. The order p denotes the number of previous values used for the approximation of the present value and $E(n) \in \mathbb{R}^{D\times N}$ being a D-dimensional Gaussian process with zero mean.

For the model approximation, we applied the state-of-the-art multivariate Kalman Filter algorithm as proposed in [38]. Unlike other MVAR estimation approaches, the K multiple trials do not have to be aggregated before or after model estimation. For multi-trial data, this algorithm has proven to be the best choice as compared to other Kalman approaches [39]. The order of the model p, i.e. number of prior time steps that are included for the current model approximation was chosen under consideration of Akaike's and Bayesian information criterion [36,40]. Under further consideration of estimated tvMVAR spectra as compared to the model-free Fourier spectra the model order was set to $p = 20$ [32].

Based on the derived model coefficients, we quantified functional relationships within the networks by means of time-variant partial directed coherence (tvPDC). It is a method which is based on the Fourier transform of the tvMVAR model parameters, to provide a frequency-selective, time-variant directed quantification of connectivity strength within the network [41]. It is important to emphasize that the quantification of weighted EEG network edges is derived from a time-series analysis based on time-variant tvMVAR modeling rather than from raw time series data.

The Fourier transformed model parameters at time point n and frequency f is calculated by $\mathbf{A}(n, f) = \sum_{r=1}^{p} A^r(n)e^{−2\pi ifr}$ [37]. Let $\bar{\mathbf{A}}(n, f) := \mathbb{1}_D − \mathbf{A}(n, f)$ with the $D \times D$ identity matrix $\mathbb{1}_D$, then the tvPDC at time point n and frequency f from network node j to i is defined as

$$\pi_{i\leftarrow j}(n, f) := \frac{|a_{ij}(n, f)|}{\sqrt{\sum_{d=1}^{D} |a_{dj}(n, f)|^2}} \in [0, 1], i \neq j$$

with $a_{ij}(n, f)$ denoting the (i, j)-th entry of $\bar{\mathbf{A}}(n, f)$. The value $\pi_{i\leftarrow j}(n, f)$ denotes the strength of connectivity from source node j to sink node i and can range from 0 (no connection) to 1 (strong connection). In practice all tvPDC values are > 0, consequently the graph of EEG network nodes with tvPDC network edges represents a fully connected graph.

From a mathematical perspective, the complete tvPDC data set thus represents a three-dimensional tensor covering the modes frequency $\times$ space $\times$ time and consists of $F \times D \cdot (D − 1) \times N − 1$ values. In this work, frequency range for tvPDC analysis was set to 0–25 Hz with a resolution $F = 50$ frequency bins, the EEG setup contained $D = 28$ active electrodes and for each trial 201 samples in time were recorded (corresponding to a time interval of 1.6 ms). That means, finally the dimensionality of the tensor that has to be visualized in this application is $F \times D \cdot (D − 1) \times N − p = 50 \times 28 \cdot 27 \times 201 − 20$. In the context of network analysis, this tensor contains the values of frequency- and time-dependent adjacency matrices where rows represent sink edges and columns the source edges. The entries of this matrix themselves contain the weights (i.e. tvPDC values) of the directed edges between the nodes. The diagonal entries of these matrices are set to zero, because self-connected nodes do not exist in the networks. Maintaining these zero entries for further processing leads to a symmetrical memory layout which will be described in the implementation Section 4.
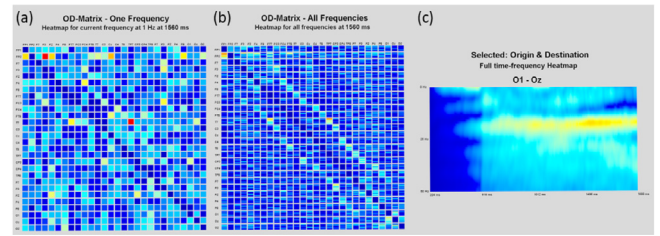
Fig. 2. Extract of the adjacency matrix heatmap panel. Subfigure (a) is restricted to one time point and one frequency. In (b) the time is fixed, the frequency varies. The time–frequency map in (c) shows the color-coded tvPDC values between the currently selected directed channel combination O1 → Oz.
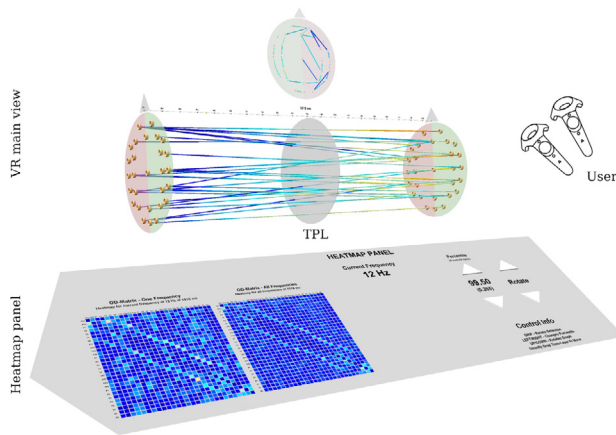
3.2. Visualization of brain connectivity in VR

As already mentioned in the introduction, many applications require a visualization that comprises *all* electrodes of the scalp that have been recorded. A basic possibility for visualizing the complete network is a color-coded adjacency matrix drawn for a certain time point and/or frequency (Fig. 2(a)). To include more information, all frequency-variant maps can be displayed in a single, large adjacency matrix. This is illustrated in Fig. 2(b), where color-coded tvPDC values vary across frequencies along the vertical axis of each cell. Although these views give a good overview of general network patterns within the brain, they do not provide detailed information about connectivity with respect to time and frequency in combination. Fig. 2(c) shows an example of a directed connection between two prechosen electrodes (O1 → Oz) which includes also the changes over time (drawn across x-axis).

Yet, none of these views combine all modes of the 4D tensor and notably also neglect the spatial arrangement of EEG electrodes across the scalp. For that reason, we propose to combine and link several different visualization techniques that jointly cover all modes of the tensor. The view we offer to the user is shown in Fig. 3. In the main view (upper row), a 3D anatomical depiction of the electrode network is provided: The *full time extended connectivity graph* (FTXC) covers the whole time interval and preserves the anatomical arrangement. It is combined with the 2D *time-selective connectivity* (TSC) representation on the very top, giving a detailed spatially arranged view of the network at a certain time point. This anatomic view is supplemented by a conventional *heatmap panel* showing the complete adjacency matrix in detail. Every entry of this matrix provides a time–frequency map corresponding to one sink and one source electrode, where the strength of connections is encoded by color. The view on all panels are synchronized upon user interaction.

In the following, we give a detailed description of the components of our visualization shown in Fig. 3. We start with a brief discussion on the chosen color mapping. This is followed by the introduction of the VR main view with the anatomically arranged view of the network. Finally, the heatmap panel with the detailed view on the corresponding adjacency matrices of the network will be described. A video demonstrating the system in action is provided in supplemental material S1.

Color mapping. Mapping numerical values to colors is a common process in scientific visualizations. A predefined color scheme is used to convert scalar values to the corresponding colors. In this application, such color mappings are necessary to visualize the connectivity strengths of the edges as well as for multiple heatmap depictions [42]. By default, the rainbow color map *Jet* is chosen, as it is the most commonly used color scale in neuroscience and known to the domain experts from widely used brain connectivity analysis tools. EEGlab [43] offers *Jet* by

Fig. 3. Virtual visual analysis lab. This is the view provided to user in VR. Interactions are possible through grabbing and pointing design to motivate interactive exploration of brain connectivity data. The VR main view shows the functional connectivity in the anatomical arrangement. Every tube represents the temporally varying connectivity from the source electrode on the left and the corresponding sink electrode. The heatmap panel represents the same network in a more abstract fashion: In the two adjacency matrices, every entry represents a directed connection between sink (matrix rows) and source (matrix columns) nodes.

Fig. 4. VR main view with selected EEG electrode. In (a), the connections are displayed in form of a 2D head. It shows the network at the time point which is chosen by time pick layer in (b).

default and very similar custom rainbow color maps are used in SIFT [44] and MELODIC [45].

Previous work on color scales [46–48] points out two drawbacks of rainbow color scale and specifically of the *Jet* color scale, though. Firstly, perceived luminance, i.e. lightness, varies in a none monotonous way. Secondly, perceived color gradients are not uniform. On the other hand, Reda et al. showed recently in [49] that rainbow color scales yield the best performance for the graphical comparison of scalar fields. They attribute this to the large number of colors with different names that are traversed in a rainbow color scale and introduce *color name variation* as a metric. In our immersive visual analysis approach color mapping is applied to thin illuminated tubes and heat map panels without illumination. In both cases lightness variations in the color scale do not affect our visualizations in a negative way (cf. Fig. 3) as pointed out for general 3D data visualization in [50]. Uniform color gradient perception is neither of high importance for color mapped tubes and heat map panels. Efficient comparison of the behavior of connectivity strengths along tubes and inside of heat map panels on the other hand is very important in our brain connectivity analysis to visually extract patterns from the data. Therefore, color name variation was more important to us than uniform lightness and monotonous gradient perception such that we preferred the use of the *Jet* color scale.

VR main view: full time extended connectivity graph. For every time step in every frequency there exists a whole asymmetric OD matrix, i.e. a fully connected directed graph, in which each edge encodes its connectivity value. In EEG research, it is common to reduce the 3D coordinates of the electrodes around the scalp into 2D coordinates resulting in a plane representation of all electrodes [51]. The ellipsoid-shaped plane represents the head viewed from above with a triangle symbolizing a nose to quickly identify the orientation of the head. The FTXC (Fig. 4(b)) is the main graph of the visualization. It utilizes the enhanced 3D perception provided by VR environments to create a novel visualization of the brain connectivity data across the whole time interval. Traditional visualizations of these networks focus on visualizing a fixed time point and therefore cannot represent the temporal evolution of brain connectivity. In this graph, source and sink of the OD data are separated as shown in Fig. 1. A simplified
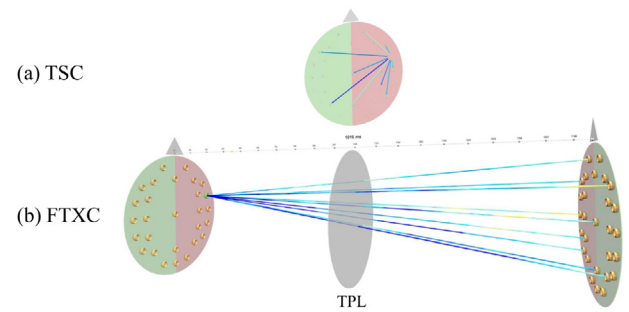
head is visualized as a disk with a triangle on top indicating the nose position, the hemispheres of the head are colored differently (green for left and red for right) to simplify interpretation of the graph from different viewing angles. Tubes connect the origin and destination electrodes for a selected frequency band. They are colored corresponding to their tvPDC value over time. Thus, the FTXC graph offers an insight into the *temporal evolution* of brain connectivity patterns.

Origin and destination electrodes can be selected to apply edge based filtering to the visualized graph. Furthermore, a time pick layer (TPL) between the origin and destination head allows the selection of a specific time step by mapping the space between the head disks to time.

The position of the time line is dynamically adjusted to not occlude the FTXC graph while being as readable as possible. For this, we consider the cylinder around the TPL connecting the source and destination head disks. Based on the tracked head position of the user, we compute the top silhouette line of the cylinder and position the time line to coincide with this.

VR main view: time-selective connectivity. In Fig. 4(a), the TPL is transferred into a node link diagram with the tvPDC values that are mapped to edge colors. While FTXC shows the entire temporal evolution of the network, moving the TPL creates and animation of the temporal network evolution in the TSC. TSC and FTXC view have the purpose to supply the user with a means of an intuitive exploration and analysis of brain connectivity. This is mainly due to the anatomical arrangement of EEG electrodes as well as to the condensation of networks to the limitation of the view on certain time and frequency points. In addition to these visualizations, a 2D heatmap panel representation was designed, showing the entire network for all electrodes, time points and frequencies at once.

Heatmap panel. A heatmap panel with the common adjacency matrices and time–frequency maps (Fig. 3, lower row) is also included into our application. These three additional representations complement the TSC and FTXC visualizations: one adjacency matrix for the current time and frequency, one adjacency matrix comprising all frequencies for the complete time interval and one time–frequency map of a predefined directed channel combination. The main purpose of this visualization is to provide a view on the time–frequency map of the selected OD edge in the VR main view. In addition, the complete network which might help to exploratively find relevant time intervals or frequency bands that should be explored in the detailed views.

3.3. User interaction

We geared all aspects of user interaction in VR towards motivating data exploration: Users interact with the visualization

Table 1

Memory footprint of main data structures and tube geometry. Note that we store two tubes per edge, one each for the FTXC and TSC graphs.

Data structure	Complexity	Data type	Size (MiB)
PDC tensor	$F \times D^2 \times T$	Float	27.07
Color texture		Float RGB	81.20
Sorted PDC list	$F \cdot D^2 \cdot T$	Float	27.07
Max-PDC array	$F \times D^2$	Float	0.15
Tube geometry	$2 \cdot F \cdot D^2 \cdot (24 + 2)$	Float vec4	31.10

via natural pointing and grabbing actions, and the virtual visual analysis lab compiling our visualizations (see Fig. 3) is sized such that users can physically walk some steps to view it from different angles.

Grabbing and pointing. The TPL has to be selected by the user in order to move it to a specific time step. Since the user has to reach the time pick layer to grab it, it encourages moving into the 3D scene and viewing the graph from different perspectives.

Electrodes can be selected to apply a spatial filter based on the selected origin and destination electrodes. This is shown in Fig. 3(a) and 4: While in Fig. 3(a) all network edges are displayed, Fig. 4 exclusively shows the connection from the chosen source electrode (in this example, electrode FT8). In contrast to the TPL, the electrodes are small. Furthermore, the origin and destination electrodes are far away. Therefore, a pointing interaction using a ray emanating form the controller tip is offered to the user in order to prevent fatigue from moving back and forth while selecting different origin and destination electrodes.

In the heatmap panel, it is possible to point to and select a certain directed channel combination from the adjacency matrices. A detailed time–frequency heatmap of the tvPDC values is then shown as a third view on the data and the corresponding electrodes are selected in the FTXC/TSC graphs. An example is given in Fig. 2, where (c) shows the connection from electrode O1 to Oz. All time points are included (x axis), as well as the whole frequency range (y axis).

Additional controls. More abstract parameters are realized as control elements directly on the heatmap panel. There, users can adjust the frequency of interest for the FTXC/TSC graphs and the single-frequency OD matrix, as well as the percentile for tvPDC threshold filtering of network edges. In Fig. 3(b) for example, the frequency is set to 10 Hz and only connections higher than 90% of all tvPDC values are displayed.

Finally, not all parameters of the visualization can or should be exposed inside the VR environment. We relegate more obscure settings relating e.g. to scene geometry or renderer properties to a traditional GUI. It offers controls for all available parameters that can be tuned by the user.

4. Implementation

To prototype the visualization for the user study, we built upon our in-house C++/OpenGL visualization framework [52]. The concept only requires fairly standard rendering and architecture — yet, a few noteworthy design decisions were made in the implementation to quickly achieve a working prototype. In the interest of reproducibility, we want to give a brief rundown of them in this section.

Data management. For the purpose of our visualization, a single loadable data set consists of the full tvPDC tensor from one individual, plus electrode definitions (position and label). We represent the tensor as a dense time-major 3D array of dimensions $F \times D^2 \times T$, where $T = N - p$ refers to the effective number of time steps in the data without model bootstrapping. Edges connecting an electrode with itself are not removed to keep the memory

layout symmetrical. Instead, we set the corresponding PDC values to 0 leading to D^2 entries in the spatial mode rather than $D(D-1)$.

We pre-compute the *Jet*-mapped colors and store them in a second 3D array of identical structure. We decided against on-the-fly color mapping because it stays constant for a single data set, while using the GPU texturing units becomes very straightforward (see *graph rendering* below).

During data import, we also create and keep a sorted list of PDC values over all frequencies and time steps. This enables efficiently determining the global coherence threshold from a percentile (in $O(1)$ time) and vise-versa (in $O(\log n)$ time), maintaining interactivity when either is changed by the user. Finally, we store the largest PDC value per graph edge and frequency to quickly filter out whole edges that exhibit no coherence above the selected threshold.

The raw data set sizes generated by the tvPDC analysis for typical EEG studies easily allow for this generous usage of memory — see Table 1 for the memory footprint of the main data structures and Fig. 5(a) for an illustration of their layout.

Graph rendering. All geometry is created during scene initialization, including the tubes representing the OD edges in the FTXC and TSC graphs. For rendering, the tubes are tessellated as cap-less cylinders using one triangle strip per connection. For the FTXC graph, the cylinders are clipped by the two head planes. We use 12 segments for the cylinder cross section, which is sufficient to make the tessellation visually indiscernible under normal use.

Again, in order to simplify indexing, we also keep all edges that connect an electrode to itself. While they would be filtered out under normal circumstances anyway due to their PDC value of 0, we create degenerate triangle strips for them in order to guarantee that the corresponding tubes are never visible.

Tube color is being applied in the fragment shader by texturing. We transfer the result of the color mapping to a 3D texture, and select the proper color series by fixing the v texture coordinate per tube such that it corresponds to the correct graph edge slice. The selected frequency is provided to the shader as a uniform variable and converted to the u coordinate for the texture lookup. w varies along the tube from 0 to 1, resulting in smooth color interpolation between time steps. This requires additional care for the FTXC graph: The color gradient should always be aligned with the time axis rather than the cylinder axis (see Fig. 5(b)). To ensure this, we project the vector from origin to destination head planes (which exactly corresponds to the time axis in VR world space) onto the tube, yielding the desired w parametrization.

To apply the threshold/percentile filtering, we compile the indices of non-filtered connections using the pre-computed maximum PDC values per graph edge and frequency, creating a batch of tubes to render in a single draw call.

Heatmap panel rendering. The OD adjacency matrix overlays consist of individual quads per cell. Their positions indirectly encode the edge index, which can be used to select the appropriate v slice from the 3D color texture. For the single frequency OD matrix, u and w are fixed and provided to the shader via uniforms according to the current frequency and time user selections, respectively. For the all-frequencies OD matrix, each quad receives the u texture coordinate as a vertex attribute such that it vertically varies from 0 to 1, w is again dependent on the user-selected time and provided in a uniform variable.

The time–frequency heatmap is rendered as a single quad with u and w texture coordinates varying along the vertical and horizontal edges, respectively. Here, the v slice depends on the user-selected electrodes.

VR Interaction. We exclusively use controller touchpad events for triggering an interaction with the scene, as we found that the resulting smaller forces on the controller improve pointing precision.
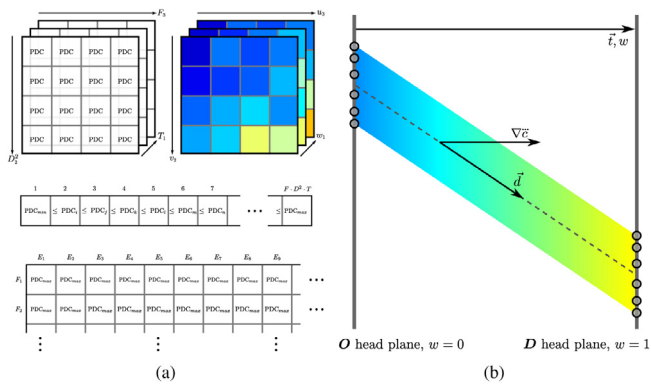
Fig. 5. (a) Main data structures. Top row: 3D arrays storing the full tvPDC tensor and pre-computed *Jet*-colors. The subscripts in the arrow labels indicate storage order. Middle and bottom row: sorted list of all PDC values and 2D array of maximum PDC values per edge and frequency. **(b) Setup of tubes in FTXC graph.** The vertices of the cylinder mantle lie on the two head planes. Setting their w texture coordinates to 0 and 1 respectively yields a world-space color gradient $\nabla \vec{c}$ that is aligned with the time axis $\vec{t}$ rather than the tube axis $\vec{d}$.

Controller point-and-select interaction is implemented by performing intersection tests of the controller rays with the oriented bounding boxes of all interactive scene objects whenever a controller pose changes. This brute-force approach is provided as-is by the underlying framework, and we found that the low number of interaction points in our lab scene made an acceleration data structure unnecessary. Grabbing-and-pointing of the TPL uses the oriented controller bounding box instead of a ray.

Additionally, we mapped several more user-settable parameters to various controller buttons. Most notably, selected frequency and the PDC threshold are adjustable using the controller directional pad.

5. Evaluation

5.1. Evaluation strategy

In a first qualitative user study, the overall experience and usability of the application have been evaluated. The VR application was tested with an HTC Vive Pro and two HTC Vive Controllers. A group of six male experts was included to test and evaluate the application. Three of them were Ph.D. students in the research field of clinical neuropsychology all working directly with EEG data. One participant was a neuroscientist researching on EEG network analysis in experimental psychological settings and is especially familiar with brain connectivity networks and their evaluation. Another participant was a psychologist working on EEG evaluations and one was an electrical engineer developing data-driven processing methods to predict EEG-based activity behaviors. The other three participants were computer scientists, being not familiar with research on brain connectivity. They were chosen to give feedback from a technical and usability point of view. Two of them were working in the field of computer graphics and had experience with VR. One participant was a front-end developer with experience in user interface design [53]. For convenience, the two groups are denoted by *neuro experts* and *VR experts* in the following.

In the beginning, the participants were briefly introduced to the basics of brain connectivity and to the tvPDC data set. This was especially necessary for the participants who were not familiar with the field of neurophysiological research. Consequently, the duration of this pre-training depended on individual participants. A non-VR time–frequency OD matrix of causal connectivity data (as shown in Fig. 2(c)) was presented and described as one

current existing solution. This should help the users to understand the visualizations in the heatmap panel. Furthermore, VR application was explained, including all displayed components and possible user interactions. This was especially important for those participants who were not familiar with the usage of VR equipment. It was clarified that all parts of the application have been understood.

After this introduction, the participants entered the virtual environment to test the application. They were instructed to consistently report what they want to achieve, what they are doing, what they had expected to happen and what actually happened (thinking-aloud method [54]). This short warming-up phase was aimed to give the participants the possibility to get used to the general virtual environment and the controllers.

Then, the test phase started. During that part, the new application should be used for exploring the calculated EEG brain networks (see paragraph 3.1). For that purpose, the participants had to perform 14 tasks covering three aspects:

- *Interaction.* Example: "Move the TPL. Observe and describe the effects it has".
- *Spatial recognition.* Example: "Pick a point on an edge of your choice in the middle of the graph. Follow the edge to determine its origin and destination".
- *Heatmap panel.* Example: "Use the All-Frequencies OD Matrix and move through time to look for interesting connectivity values in other frequencies".

The set of tasks was designed in such way that the participants were faced with all aspects considered in the final questionnaire at least once during that phase. In the supplementary material S2, a list of all devised tasks can be found.

Finally, the participants were asked to fill a questionnaire (supplementary material S3) where they had to respond how much they disagree or agree with each statement on a five-level Likert scale [55]: strongly disagree (1), disagree (2), neither (3), agree (4) and strongly agree (5). The statements randomly alternate between positive and negative expressions so that the respondent had to read each statement carefully and make an effort to think whether to agree or disagree. For analysis and visualization, the ratings of these alternating items were finally transferred to the converted Likert scale. This transformation converts the participants' ratings of negative expressions into the equivalent rating value for the according positive expression by subtracting the negative rating from 6. As an example: If a participant strongly disagrees (1) with the negative expression "I did not feel encouraged to make use of the time-pick-layer.", the value is converted into $6 - 1 = 5$, meaning that the participant strongly agrees (5) with the corresponding positive expression "I felt encouraged to make use of the time-pick-layer.".

The first part of the questionnaire (supplementary material S3) covered the overall experience of the VR visualization as compared to the inspection of non-VR time frequency adjacency matrices. This was followed by more detailed questions concerning the TPL, the 2D graph and the heatmap panel. Finally, ten items assessing the system usability scale (SUS) [56,57] were used to receive a global assessment of the system's usability. To obtain a qualitative assessment of the usability, the answers to the SUS questionnaire are used to obtain a general grading scale [58,59]. First, the Likert scale SUS results are converted into the SUS score reaching values between 1 and 100. The SUS score is then transformed into an ordinate rating scale, ranging from *A+* to *F*, which provides an intuitive impression about the general usability of a tool in form of a letter grade.

Table 2

SUS statements and results from the user study questionnaire. Mean, standard deviation (SD) and median across subjects are listed for each statement. Positive statements are displayed in green, negative in red. Agreement of participants are encoded via a five-level Likert scale: strongly disagree (1), disagree (2), neither (3), agree (4) and strongly agree (5).

Statement	Mean	SD	Median
24. I think that I would like to use this system frequently.	4.0	0.00	4
25. I found the system unnecessarily complex.	2.0	0.58	2
26. I thought the system was easy to use.	4.2	0.37	4
27. I think that I would need the support of a technical person to be able to use this system.	1.7	0.47	2
28. I found the various functions in this system were well integrated.	3.7	0.47	4
29. I thought there was too much inconsistency in this system.	2.0	0.00	2
30. I could imagine that most people would learn to use this system very quickly.	3.5	0.96	3.5
31. I found the system very cumbersome to use.	1.7	0.47	2
32. I felt very confident using the system.	4.2	0.69	4
33. I needed to learn a lot of things before I could get going with this system.	2.3	0.94	2
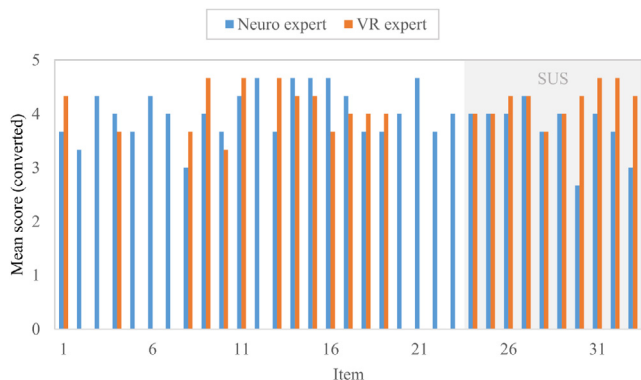
Fig. 6. Mean questionnaire results. For every questionnaire item 1, . . . , 33 the two colored bars represent the mean Likert scale value (mean across each expert group). Several questions had only to be answered by participants with a related neurophysiological background. The gray box highlights the ten SUS items at the end of the questionnaire.

5.2. Results

In this section, we present a summary of basic evaluation results. Due to the small group size of six participants, all reported results are based on descriptive statistics and do not include any inferential statistics drawn from hypothesis testing. The answers of the participants to the complete questionnaire including the SUS items are listed in the supplementary material S4. Note that the table provided S4 contains raw ratings rather than derived values based on converted Likert scale.

To provide a rough overview about general assessment of neuro expert group vs. VR expert group, Fig. 6 shows a bar plot of converted Likert scale values covering all answers to the 33 questionnaire items (mean across each group). The last ten items contain the SUS-related questions, highlighted by a gray box. At first glance, the ratings of the neuro expert group seem lower and more broadly spread than those of the VR experts. This is confirmed by the group-dependent overall mean (mean$_{neuro}$: 3.98, mean$_{VR}$: 4.33) and standard deviation (SD$_{neuro}$: 0.74, SD$_{VR}$: 0.64). Interestingly, for the neuro expert group, the items related to the application which had only to be answered by the neuro experts have been rated slightly higher (mean: 4.07) than the more general items (mean: 3.88).

General feedback. In general, the new visualization concept received positive feedback: Five out of six participants agreed or strongly agreed with liking the overall experience (mean: 4.00, SD: 1.0). The users think that the visualization is suited for analyzing functional connectivity data in a professional context (mean: 4.33, SD: 0.47) and compared to a non-VR OD matrix the application gives a better complete overview of the data (mean: 4.33, SD: 0.47). The question whether the visualization generally

motivates them to analyze and explore the data further is scored in the middle area (mean=3.33, SD: 0.47). Yet, compared to a non-VR OD matrix they feel more motivated to further explore the network and reported that the detailed view in the heatmap panel provides a beneficial complement.

FTXC, TPL, TSC. Compared to a time–frequency view of all adjacency matrices, all but one agreed that identifying the spatial context of connectivity after seeing an interesting color is easier with the TXC Graph solution (mean: 3.83, SD: 0.90). They furthermore agree or strongly agree that the strength of connectivity is well-presented by the chosen color map (mean: 4.67, SD: 0.47) and think that the connectivity information is perceived in a more detailed way regarding temporal resolution (mean: 4.33, SD: 0.47). Most participants reported that it was not easy to distinguish between the edges within when the fully connected graph was drawn, or the threshold for the drawn edges was set very low (mean: 3.33, SD: 0.75).

The additional time-selective filtering option (time pick layer) received positive feedback, especially corresponding to the time point of the visual stimulus. In general, neuro experts gave some more thoughts about the usage in a professional context than the computer scientists. All participants considered the TSC Graph as helpful, while the opinions varied concerning the question whether the graph improves the identification of spatial relations between connected electrodes.

Regarding some controller interactions, it was observed that initially multiple users without any VR experience had trouble finding the grip key to undo the electrode selection and tapping the touchpad instead of pressing it. Furthermore, most users tried to point and select the TPL instead of directly moving it. All these issues were resolved after the interactions were executed correctly once. These initial problems could be related to the mentioned scores at the end of the system usability passage of this section. It was also observed that when users were unsure about key mappings they did not seem to look at the interaction control overview printed on the heatmap panel.

Heatmap panel. The heatmap panel and the additional heatmap representations were perceived as a useful extension of the FTXC Graph and especially well suited for exploratory data analysis. All experts found the single edge time–frequency heatmap very useful (mean: 4.66, SD: 0.47). The *One-Frequency OD Matrix* (mean: 4.00, SD: 0.82) and the *Electrode Selection Heatmap* (mean: 4.00, SD: 0.82) also received positive response. Five out of six participants liked the general position of the heatmap panel (mean: 3.83, SD: 0.37). It has though been criticized that the panel is too big to receive a general overview from all positions in space, especially for analyzing OD matrices while moving the TPL to the end of the time line.

System usability.

Table 2 lists the Likert scale mean, standard deviation (SD) and median of the SUS questionnaire across the whole group.
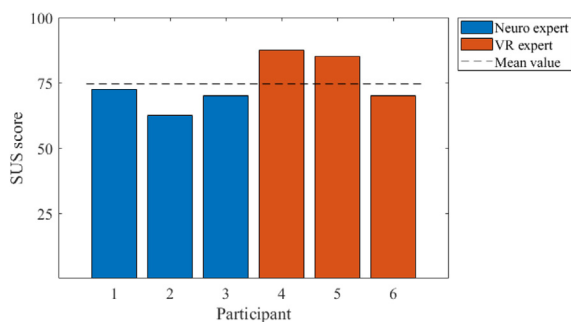
Fig. 7. SUS score of each participant. The bars represent the individual assessment regarding the general experience of the new tool. The neuro expert group reported a usability slightly below the overall average of SUS scores (74.58), while two of three VR experts assess the tool better as compared to the group mean.

All participants agreed that they would like to use this system frequently (mean: 4.0, SD: 0.00). The individual ratings can be found in the last ten rows of the table in supplementary material S4. Unnecessary complexity (mean: 2.0, SD: 0.58) was rated low and easiness to use (mean: 4.2, SD: 0.37) was rated high. Notably, participants with prior experience in VR stated the highest SUS values.

Two statements that produced controversial results are the items: "I would imagine that most people would learn to use this system very quickly." (mean: 3.50, SD: 0.96) and "I needed to learn a lot of things before I could get going with this system." (mean: 2.33, SD: 0.94). Both relate to the initial introduction phase. The participants with VR experience rated these statements very positively while two of the brain activity experts gave a more moderate feedback.

Fig. 7 shows the resulting SUS score for each participant. The SUS scores range from minimum 62.50 to maximum 87.50 with an overall mean of 74.58 which represents a *good* system usability (letter grade *B*). According to [60], this SUS value indicates a system usability considerably above the average of other studies which is 68.

6. Discussion and conclusion

For our user study, we included experts from the field of EEG data analysis as well as computer scientists. The results yield positive feedback for exploratory data analysis especially in the use case of non hypothesis-driven research. Participants liked the overall experience and experts with background in brain activity analysis think it would be helpful using this application in a professional context. This indicates that an immersive 3D view of anatomically arranged brain offers a support for a data-driven, intuitive exploration of temporally varying, multi-dimensional brain networks.

So far our proof of concept study includes a small group of six participants which merely allows a descriptive analysis of given feedback. In our future work, we will considerably increase the group size and investigate whether the application might significantly help for the visual analysis and comparison of brain networks between several subjects, groups or experimental tasks. Another open question is: To what extent does the VR view help to better understand network patterns in comparison to a 3D desktop view? Here, simulated time series with predefined network patterns (ground truth) are helpful to evaluate and quantify the benefit of the VR approach in a user study.

A basic shortcoming is the occurring visual clutter with increasing number of displayed network nodes and the connection lines between origin and destination electrodes in 3D. As

described, several filtering options have been implemented to counteract this drawback and give the user the possibility to apply a tvPDC threshold for visible connections (according to time, frequency and tvPDC threshold) as well as a deliberate selection of electrodes. Nevertheless, a main objective of future work will be to find ways to reduce visual clutter in order to display more edges simultaneously. This may for example include utilizing transparency for low-valued parts of the edges as well as edge-layouting techniques.

In conclusion, the user study indicates that the anatomical arrangement in combination with the TPL provides an intuitive view which turns out to be better understandable than the time–frequency adjacency matrix representation. User feedback indicates that this aspect in particular greatly benefits from the immersive setting, as participants were easily able to understand the graph spatially and could interact with it in a way that felt natural to them. Most notably, this application allows the exploration of the whole network with all involved modes at once, instead of focusing on a hypotheses-driven preselection of brain regions of interest, relevant time intervals or frequency bands.

CRediT authorship contribution statement

Britta Pester: Conceptualization, Methodology, Formal analysis, Writing – Original draft, Visualization. **Benjamin Russig:** Software, Writing – original draft, Visualization. **Oliver Winke:** Conceptualization, Methodology, Software, Formal analysis, Visualization. **Carolin Ligges:** Investigation, Writing – review & editing. **Raimund Dachselt:** Supervision. **Stefan Gumhold:** Writing – review & editing, Supervision.

Declaration of competing interest

The authors declare that they have no known competing financial interests or personal relationships that could have appeared to influence the work reported in this paper.

Acknowledgments

Appendix A. Supplementary data

Supplementary material related to this article can be found online at https://doi.org/10.1016/j.cag.2022.05.024.

References

[1] Yeung AWK, Goto TK, Leung WK. The changing landscape of neuroscience research, 2006–2015: a bibliometric study. Front Neurosci 2017;11:120.

[2] Babiloni C, Lizio R, Marzano N, Capotosto P, Soricelli A, Triggiani AI, et al. Brain neural synchronization and functional coupling in Alzheimer's disease as revealed by resting state EEG rhythms. Int J Psychophysiol 2016;103:88–102.

[3] Liao W, Zhang Z, Pan Z, Mantini D, Ding J, Duan X, et al. Altered functional connectivity and small-world in mesial temporal lobe epilepsy. PLoS One 2010;5(1).

[4] Ligges C, Ungureanu M, Ligges M, Blanz B, Witte H. Understanding the time variant connectivity of the language network in developmental dyslexia: new insights using Granger causality. J Neural Trans 2010;117(4):529–43.

[5] Fingelkurts AA, Fingelkurts AA, Kähkönen S. Functional connectivity in the brain - is it an elusive concept? Neurosci Biobehav Rev 2005;28(8):827–36.

[6] Pfister H, Kaynig V, Botha CP, Bruckner S, Dercksen VJ, Hege H-C, et al. Visualization in connectomics. In: Scientific visualization. Springer; 2014, p. 221–45.

[7] Garces P, Pereda E, Hernández-Tamames JA, Del-Pozo F, Maestu F, Ángel Pineda-Pardo J. Multimodal description of whole brain connectivity: A comparison of resting state MEG, fMRI, and DWI. Human Brain Mapp 2016;37(1):20–34.

[8] Chang C, Chen JE. Multimodal EEG-fMRI: advancing insight into large-scale human brain dynamics. Curr Opin Biomed Eng 2021;18:100279.

[9] Wirsich J, Amico E, Giraud A-L, Goñi J, Sadaghiani S. Multi-timescale hybrid components of the functional brain connectome: A bimodal EEG-fMRI decomposition. Netw Neurosci 2020;4(3):658–77.

[10] Sakkalis V. Review of advanced techniques for the estimation of brain connectivity measured with EEG/MEG. Comput Biol Med 2011;41(12):1110–7.

[11] Blinowska KJ, Rakowski F, Kaminski M, Fallani FDV, Del Percio C, Lizio R, et al. Functional and effective brain connectivity for discrimination between Alzheimer's patients and healthy individuals: A study on resting state EEG rhythms. Clin Neurophysiol 2017;128(4):667–80.

[12] Fortunato S, Hric D. Community detection in networks: A user guide. Phys Rep 2016;659:1–44.

[13] Pester B, Winke O, Ligges C, Dachselt R, Gumhold S. Immersive 3D visualization of multi-modal brain connectivity. In: EuroVis workshop on visual analytics. The Eurographics Association; 2021.

[14] Kuhlen TW, Hentschel B. Towards an explorative visual analysis of cortical neuronal network simulations. In: International workshop on brain-inspired computing. Springer; 2013, p. 171–83.

[15] Harris RL. Information graphics: A comprehensive illustrated reference. Oxford University Press; 2000.

[16] Jenny B, Stephen DM, Muehlenhaus I, Marston BE, Sharma R, Zhang E, et al. Design principles for origin-destination flow maps. Cartogr Geogr Inf Sci 2018;45(1):62–75.

[17] Boyandin I, Bertini E, Bak P, Lalanne D. Flowstrates: An approach for visual exploration of temporal origin-destination data. In: Computer graphics forum. Vol. 30, Wiley Online Library; 2011, p. 971–80.

[18] Yang Y, Dwyer T, Goodwin S, Marriott K. Many-to-many geographically-embedded flow visualisation: An evaluation. IEEE Trans Vis Comput Graphics 2016;23(1):411–20.

[19] Kwon O-H, Muelder C, Lee K, Ma K-L. A study of layout, rendering, and interaction methods for immersive graph visualization. IEEE Trans Vis Comput Graphics 2016;22(7):1802–15.

[20] Czauderna T, Haga J, Kim J, Klapperstück M, Klein K, Kuhlen T, et al. Immersive analytics applications in life and health sciences. In: Immersive analytics. Springer; 2018, p. 289–330.

[21] Büschel W, Vogt S, Dachselt R. Augmented reality graph visualizations. IEEE Comput Graph Appl 2019;39(3):29–40.

[22] Cordeil M, Cunningham A, Dwyer T, Thomas BH, Marriott K. ImAxes: Immersive axes as embodied affordances for interactive multivariate data visualisation. In: Proceedings of the 30th annual ACM symposium on user interface software and technology, 2017. p. 71–83.

[23] Prouzeau A, Lhuillier A, Ens B, Weiskopf D, Dwyer T. Visual link routing in immersive visualisations. In: Proceedings of the 2019 ACM international conference on interactive surfaces and spaces, 2019. p. 241–53.

[24] Yang Y, Dwyer T, Jenny B, Marriott K, Cordeil M, Chen H. Origin-destination flow maps in immersive environments. IEEE Trans Vis Comput Graphics 2018;25(1):693–703.

[25] Drogemuller A, Cunningham A, Walsh J, Cordeil M, Ross W, Thomas B. Evaluating navigation techniques for 3d graph visualizations in virtual reality. In: 2018 international symposium on big data visual and immersive analytics (BDVA). IEEE; 2018, p. 1–10.

[26] Kraus M, Weiler N, Oelke D, Kehrer J, Keim DA, Fuchs J. The impact of immersion on cluster identification tasks. IEEE Trans Vis Comput Graphics 2019;26(1):525–35.

[27] Keiriz JJ, Zhan L, Chukhman M, Ajilore O, Leow AD, Forbes AG. Exploring the human connectome topology in group studies. 2017, arXiv preprint arXiv:1706.10297.

[28] Keiriz JJ, Zhan L, Ajilore O, Leow AD, Forbes AG. Neurocave: A web-based immersive visualization platform for exploring connectome datasets. Netw Neurosci 2018;2(3):344–61.

[29] Pester B, Ligges C, Leistritz L, Witte H, Schiecke K. Advanced insights into functional brain connectivity by combining tensor decomposition and partial directed coherence. PLoS ONE 2015;10(6):e0129293.

[30] Acharya JN, Hani AJ, Cheek J, Thirumala P, Tsuchida TN. American clinical neurophysiology society guideline 2: Guidelines for standard electrode position nomenclature. Neurodiagnostic J. 2016;56(4):245–52, PMID: 28436791.

[31] Sazgar M, Young MG. Overview of EEG, electrode placement, and montages. In: Absolute epilepsy and EEG rotation review: essentials for trainees. Springer International Publishing; 2019, p. 117–25.

[32] Pester B. Novel approaches for exploring highly resolved brain connectivity: development, evaluation and practical application. (Ph.D. thesis), Friedrich-Schiller-Universität Jena; 2016.

[33] Tong S, Thankor NV. Quantitative EEG analysis methods and clinical applications. Artech House; 2009.

[34] Piciucco E, Maiorana E, Falzon O, Camilleri KP, Campisi P. Steady-state visual evoked potentials for EEG-based biometric identification. In: 2017 international conference of the biometrics special interest group (BIOSIG). IEEE; 2017, p. 1–5.

[35] Bressler SL, Tang W, Sylvester CM, Shulman GL, Corbetta M. Top-down control of human visual cortex by frontal and parietal cortex in anticipatory visual spatial attention. J Neurosci 2008;28(40):10056–61.

[36] Pagnotta MF, Plomp G. Time-varying MVAR algorithms for directed connectivity analysis: Critical comparison in simulations and benchmark EEG data. PLoS One 2018;13(6):e0198846.

[37] Brockwell PJ, Davis RA. Time series: theory and methods. Springer Science & Business Media; 2009.

[38] Milde T, Leistritz L, Astolfi L, Miltner WH, Weiss T, Babiloni F, et al. A new Kalman filter approach for the estimation of high-dimensional time-variant multivariate AR models and its application in analysis of laser-evoked brain potentials. NeuroImage 2010.

[39] Ghumare E, Schrooten M, Vandenberghe R, Dupont P. Comparison of different Kalman filter approaches in deriving time varying connectivity from EEG data. In: 2015 37th annual international conference of the IEEE engineering in medicine and biology society (EMBC). IEEE; 2015 p. 2199–202.

[40] Schwarz G. Estimating the dimension of a model. Ann Statist 1978;461–4.

[41] Baccalá LA, Sameshima K. Partial directed coherence: a new concept in neural structure determination. Biol Cybernet 2001;84(6):463–74.

[42] Stauffer R, Mayr GJ, Dabernig M, Zeileis A. Somewhere over the rainbow: How to make effective use of colors in meteorological visualizations. Bull Am Meteorol Soc 2015;96(2):203–16.

[43] Delorme A, Makeig S. EEGLAB: an open source toolbox for analysis of single-trial EEG dynamics including independent component analysis. J Neurosci Methods 2004;134(1):9–21.

[44] Mullen T. Source information flow toolbox (SIFT). Swartz Center Comput Neurosci 2010;1–69.

[45] Beckmann CF, DeLuca M, Devlin JT, Smith SM. Investigations into resting-state connectivity using independent component analysis. Philos Trans R Soc B 2005;360(1457):1001–13.

[46] Rogowitz BE, Kalvin AD. The "which blair project": A quick visual method for evaluating perceptual color maps. In: Proceedings visualization, 2001. VIS'01. IEEE; 2001, p. 183–556.

[47] Moreland K. Diverging color maps for scientific visualization. In: International symposium on visual computing. Springer; 2009, p. 92–103.

[48] Eddins S. Rainbow color map critiques: An overview and annotated bibliography. MathWorks Tech Articles Newslett 2014;25:92238v00.

[49] Reda K, Szafir DA. Rainbows revisited: modeling effective colormap design for graphical inference. IEEE Trans Vis Comput Graphics 2020;27(2):1032–42.

[50] Zhou L, Hansen CD. A survey of colormaps in visualization. IEEE Trans Vis Comput Graphics 2015;22(8):2051–69.

[51] Committee EPN, et al. Guideline thirteen: guidelines for standard electrode position nomenclature. J Clin Neurophysiol 1994;11:111–3.

[52] Gumhold S. The computer graphics and visualization framework. 2021, URL https://sgumhold.github.io/cgv/overview.html.

[53] Winke O. 3D visualization of multi-dimensional origin-destination brain connectivity data in an immersive virtual reality environment. TU Dresden, Chair of Computer Graphics and Visualization; 2019.

[54] Boren T, Ramey J. Thinking aloud: Reconciling theory and practice. IEEE Trans Prof Commun 2000;43(3):261–78.

[55] Joshi A, Kale S, Chandel S, Pal DK. Likert scale: Explored and explained. Br J Appl Sci Technol 2015;7(4):396.

[56] Brooke J. SUS - a quick and dirty usability scale. Usability Eval Ind 1996;189(194):4–7.

[57] Lewis JR. The system usability scale: past, present, and future. Int J Hum-Comput Interact 2018;34(7):577–90.

[58] Bangor A, Kortum P, Miller J. Determining what individual SUS scores mean: Adding an adjective rating scale. J Usability Stud 2009;4(3):114–23.

[59] Sauro J, Lewis JR. Quantifying the user experience: practical statistics for user research. Morgan Kaufmann; 2016.

[60] Sauro J. A practical guide to the system usability scale: background, benchmarks & best practices. CreateSpace Independent Publishing Platform; 2011.